Autonomous & adaptive oceanographic front tracking on board autonomous underwater vehicles

Petillo S., H. Schmidt, P.F.J. Lermusiaux, D. Yoerger and A. Balasuriya, 2015.
"Autonomous & Adaptive Oceanographic Front Tracking On Board Autonomous Underwater Vehicles."
Proceedings of IEEE OCEANS'15 Conference, Genoa, Italy, 18-21 May, 2015.

Autonomous & Adaptive Oceanographic Front Tracking On Board Autonomous Underwater Vehicles

Stephanie Petillo*, Henrik Schmidt*, Pierre Lermusiaux*, Dana Yoerger†, and Arjuna Balasuriya‡
*Department of Mechanical & Ocean Engineering, Massachusetts Institute of Technology, Cambridge, MA 02139
Email: stephanie@gobysoft.org, henrik@mit.edu, pierrel@mit.edu
†Department of Applied Ocean Physics & Engineering, Woods Hole Oceanographic Institution, Woods Hole, MA 02543
Email: dyoerger@whoi.edu
‡IntelliRobo, LLC, Acton, MA 01720
Email: arjuna@ieee.org

***Abstract*—Oceanic fronts, similar to atmospheric fronts, occur at the interface of two fluid (water) masses of varying characteristics. In regions such as these where there are quantifiable physical, chemical, or biological changes in the ocean environment, it is possible—with the proper instrumentation—to track, or map, the front boundary.**

In this paper, the front is approximated as an isotherm that is tracked autonomously and adaptively in 2D (horizontal) and 3D space by an autonomous underwater vehicle (AUV) running MOOS-IvP autonomy. The basic, 2D (constant depth) front tracking method developed in this work has three phases: detection, classification, and tracking, and results in the AUV tracing a zigzag path along and across the front. The 3D AUV front tracking method presented here results in a helical motion around a central axis that is aligned along the front in the horizontal plane, tracing a 3D path that resembles a slinky stretched out along the front.

To test and evaluate these front tracking methods (implemented as autonomy behaviors), virtual experiments were conducted with simulated AUVs in a spatiotemporally dynamic MIT MSEAS ocean model environment of the Mid-Atlantic Bight region, where a distinct temperature front is present along the shelfbreak. A number of performance metrics were developed to evaluate the performance of the AUVs running these front tracking behaviors, and the results are presented herein.

I. Introduction

Oceanic fronts, similar to atmospheric fronts, occur at the interface of two fluid (water) masses of varying characteristics (e.g., temperature, salinity, density, and/or currents). These fronts often also occur in regions of rapidly changing bathymetry, such as coastal shelfbreaks, where water from the deep ocean comes in contact with coastal waters. At these frontal interfaces there may be increases in biological activity, interesting flow patterns, convergence zones where pollutants gather, or other water property variations [1]. In particular, the meeting of two water masses at a front is an important region to study, as the difference in density between the two water masses result in vertical velocities that can cause nutrients to be cycled up from deep in the ocean. This nutrient upwelling plays a critical role in supporting biological productivity near the ocean's surface. Where there are such quantifiable physical, chemical, or biological changes in the ocean environment, it is possible—with the proper instrumentation—to track, or map, the front boundary.

In the case of a front boundary defined primarily by a locally high temperature or salinity gradient, it is possible to use a conductivity-temperature-depth (CTD) sensor to sample the front. CTD sensors can be compact enough to mount on board autonomous underwater vehicles (AUVs) and other small oceanographic platforms. Past methods for sampling along and across ocean fronts have included shipboard sampling transects, moored arrays of instruments, and remote sensing via satellites. Only recently have various robotic marine platforms been employed for this purpose. Each of these methods has benefits and drawbacks in terms of sampling resolution and efficiency, synopticity across a range of spatiotemporal scales, and resources necessary to perform sampling surveys. As described by He et al. [1], the field is moving toward employing new AUV fleets for more synoptic and persistent monitoring of certain U.S. coastal regions, such as at the Pioneer Array south of Cape Cod, MA, but the infrastructure has yet to be completed. In addition, environmentally adaptive autonomous sampling methods for the AUVs to be deployed at the Poineer Array and similar coastal nodes are not currently being considered due to the increased computational and technological complexity over preplanned transects. As a result, environmentally adaptive autonomous sampling methods are still in the development and testing phases for the smaller AUV groups. For general reviews on oceanic adaptive sampling and path planning, we refer to [2]–[11]. Related works on adaptive front tracking and onboard routing include [12]–[17].

In this paper, a couple of novel methods for environmentally adaptive autonomous sampling and tracking along an ocean front are proposed and implemented using AUVs by employing the Autonomous Adaptive Environmental Assessment (AAEA) and Feature Tracking method developed by Petillo et al. [18], [19]. AAEA is described as "a process by which an AUV autonomously assesses the hydrographic environment it is swimming through in real time. This assessment is essentially the detection of hydrographic features of interest and leads naturally to the subsequent active/adaptive tracking of a selected feature," [18].

The vehicles used for this work run the MOOS middleware and IvP Helm autonomy on board, including numerous autonomy behaviors that control the AUVs' safety, maneuvering, and sampling paths. A spatiotemporally dynamic MIT MSEAS (Massachusetts Institute of Technology Multidisciplinary Simulation, Estimation, and Assimilation Systems) [20] ocean model of the Mid-Atlantic Bight (MAB) region off the east coast of the United States is used as a testing environment for virtual experiments, allowing the evaluation of these new AUV front tracking methods.

The results from numerous AUV front tracking virtual experiments (2D) at constant depth are presented, including performance metrics comparing the adaptive front tracking to preplanned survey methods. A behavior allowing AUVs to perform 3D front tracking (to sample the front in the depth dimension, as well as the horizontal plane) is also explored, and results from virtual experiments are presented.

The specific goals here are to apply AAEA and Feature Tracking to adaptively sample along and across an ocean front using only the data collected on board an AUV, gathering a synoptic data set of the position of the front over time while improving sampling efficiency and density over current preplanned AUV sampling surveys.

Petillo S., H. Schmidt, P.F.J. Lermusiaux, D. Yoerger and A. Balasuriya, 2015.
"Autonomous & Adaptive Oceanographic Front Tracking On Board Autonomous Underwater Vehicles."
Proceedings of IEEE OCEANS'15 Conference, Genoa, Italy, 18-21 May, 2015.

II. Novel Concepts & Approach

The approach to front tracking developed here is a novel combination of the real-time adaptive autonomy approach presented by Zhang et al. [15], [16] and the along-front zigzag method presented by Cannell and Stilwell [17], resulting in two primary autonomous and adaptive front tracking methods: 2D front boundary tracking with a zigzag pattern and 3D front interface tracking with a horizontal helix pattern. Both of these methods encourage travel in the along-front direction as well as across-front mapping in real time.

Following the goals stated in Section I, the front tracking methods proposed here emphasize reduced algorithm and implementation complexity to improve robustness for deployment in field experiments in the foreseeable future. In this case, temperature changes are used as the frontal indicator due to the measurement stability and physical size of temperature sensors available for small sub-sea platforms. Temperature, unlike density, can be measured directly, and many small salinity (conductivity) sensors are sensitive to temperature changes, thus making temperature the more robust characteristic to measure.

The front tracking behaviors described here focus on tracing the front boundary with one AUV in either 2D (constant depth) or 3D space. The underlying behavior for this employs an initial survey of the area followed by a zigzagging motion (in the horizontal plane) back and forth across an isotherm, where the isotherm is detected and selected by the AUV as the temperature of the front boundary. As the AUV is collecting temperature and position data, it constantly updates the frontal isotherm temperature and the estimate of the local front position. With these continual updates, the AUV is able to adapt its motion to track the front locally, synoptically sampling along the front and maintaining coverage across the front, even as the front moves in space and time.

The single-AUV 2D (zigzag) front tracking (see inset in Fig. 1) can be directly extrapolated into 3D as a horizontal helix behavior, where the long axis of the helix is at a constant depth and aligned in the horizontal plane with the local front line estimate (see Fig. 2), as in the 2D case.

To increase spatial coverage in the (horizontal) along-front direction, multiple AUVs may be employed in a follow-the-leader fashion. Though beyond the scope of this paper, this multi-AUV follow-the-leader behavior can be coupled with either the single-AUV 2D zigzag method (Fig. 1) or the single-AUV 3D helix method mentioned above. Using multiple AUVs can provide synoptic sampling coverage over a larger spatial scale than a single AUV when the AUVs are distributed within the front's characteristic length scale of each other, as sketched in Fig. 1. Further details regarding the implementation of this multi-AUV front tracking behavior are found in Chapter 5 of [19].

Other front tracking approaches described in related literature range from theoretical simulations with AUVs to determine variation of a front's position assuming a known environment [15], [16], [22], to distributing underwater gliders within the frontal boundary of a plume [23]. The simplicity of our approach—the zigzag motion and the tracking of an isotherm rather than a temperature gradient (which may dissipate or change from one stretch of the front to another)—keeps the complexity of this autonomous and adaptive front tracking method to a minimum, which is important for reducing the possible failure modes when deploying this technology in real, dynamic ocean environments. It is also assumed that, due to computational and power limitations on real AUVs and the very limited data transfer available via acoustic communications, the AUVs will have no outside knowledge (e.g., no satellite data and no ocean models uploaded or generated on board) of the environment other than what they collect with their on-board sensors in real time. Thus, the sampling patterns the AUVs decide upon autonomously must yield enough environmental information for them to make informed decisions about where to go next to properly sample the front.

The primary drawbacks to this front tracking method reside in the cases where the AUV 'loses' the primary frontal isotherm, either 1) by the front advecting away from the AUV faster than the AUV can move or 2) by the AUV becoming stuck along a local pocket of isotherm that is greater than O(1 km) in horizontal extent (having the same temperature as the front) but is not along the primary front, such as around a slope-water eddy. The former of these cases is unavoidable—resulting from the propulsion limitations of the AUV being used—and, thus, is a problem for most front tracking methods. The latter is difficult to avoid whether tracking a front boundary based on an isotherm or an across-front gradient value, since local pockets of the temperature and temperature gradient values may occur on scales ranging up to the mesoscale, making them hard to distinguish from the primary front line when all that is available are point measurements of temperature values that are assumed to be connected into a line if they share the same isothermal or gradient value with the front. In order to reduce time the AUV spends 'lost' and account

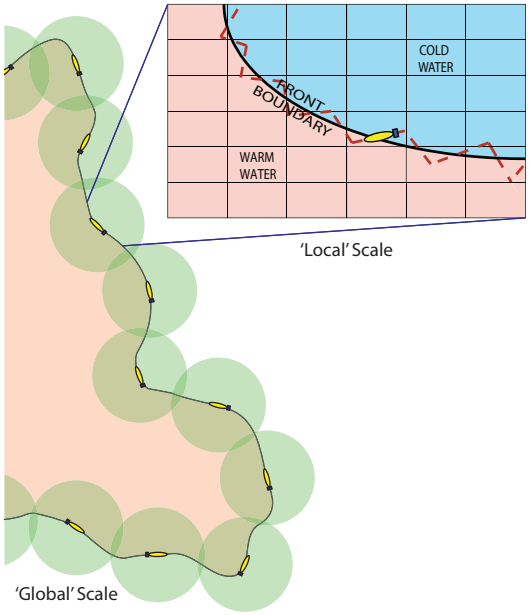

Fig. 1. A conceptual illustration of 2D single- (inset) and multi-AUV front tracking, exhibiting 'global' adaptive follow-the-leader motion of AUVs along the front and 'local' 2D adaptive zigzag motion of AUVs across the front. The green circles represent the front's spatiotemporal scales as a distance between AUVs. When these AUV range circles overlap along a front line, the sampling may be considered synoptic. Used with permission from [21].

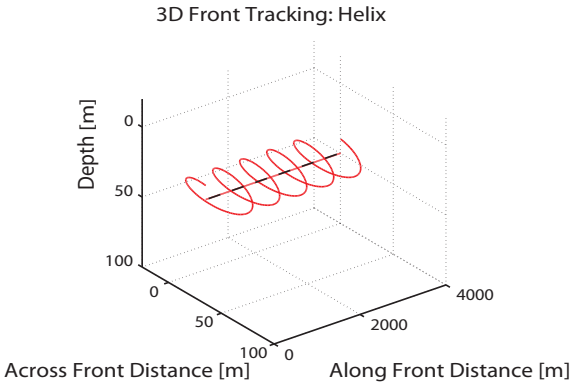

Fig. 2. A conceptual sketch of the horizontal helix pattern used for 3D front tracking. The helix's center axis is at a fixed depth, aligned with the locally estimated front boundary line (dashed straight line) in the horizontal plane.

Petillo S., H. Schmidt, P.F.J. Lermusiaux, D. Yoerger and A. Balasuriya, 2015.
"Autonomous & Adaptive Oceanographic Front Tracking On Board Autonomous Underwater Vehicles."
Proceedings of IEEE OCEANS'15 Conference, Genoa, Italy, 18-21 May, 2015.

for the significant spatiotemporal variation of temperature along the front, a timeout is included in the front tracking behaviors that restarts the front tracking process, determining a new frontal isotherm to track near the AUV's location. If an AUV is stuck in a local mesoscale temperature pocket, however, it may still re-find and remain in that pocket after a timeout. This is simply a shortcoming of front tracking methods such as this, where the AUVs determine and track the front location based on a locally sub-mesoscale sampling pattern.

Further details of the implementation and algorithms for the front tracking methods described in this section are provided in Sections III and IV.

III. 2D Front Tracking

The basic, 2D (constant depth) front tracking method developed here has three phases: detection, classification, and tracking. This is sketched out in Fig. 3. Throughout the front tracking exercise, the AUV is constantly monitoring the water temperature and updating the maximum and minimum temperature values it has encountered. In this case, the front is defined as the isotherm with the temperature half way between the max and min temperatures. It is reasonable to select an isotherm as the local front line, since isotherms often run roughly parallel to the actual high-gradient line along the front.

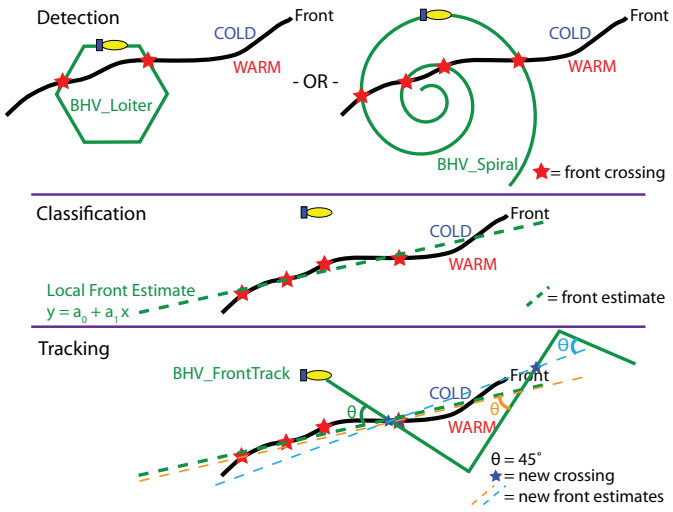

Fig. 3. The 2D (constant depth) front tracking method, which is comprised of three phases: detection, classification, and tracking.

1) Detection: The AUV performs a survey of the local region to detect the front (loiter or spiral behavior), an isotherm is selected to represent the front line, and a minimum of three front 'crossing' points are collected to trigger the classification phase.

2) Classification: The AUV estimates the local front as a line using a weighted linear least squares approximation, requiring at least three crossing points to be within a specific spatiotemporal range of the current time and AUV position to produce the linear approximation for tracking to begin.

3) Tracking: The heading of the AUV is set to intersect the front line estimate at a 45° angle. The front estimate is updated when the AUV crosses the front on that heading, and the heading required to intersect the front again (also at a 45° angle) is determined and set once the AUV has traveled a specified distance from the front. This results in a zigzag path along the front as the front shifts over space and time.

To implement 2D front tracking, the autonomy behavior BHV_FrontTrackNoBdry was developed. This behavior guides a single AUV through the detection, classification, and tracking phases, resulting in a zigzag pattern tracing the front line (isotherm), punctuated by loiter and/or spiral patterns when the front is lost or the behavior is reinitialized.

A more accurate way to detect the frontal isotherm than the averaging of min and max temperatures is to have the AUV perform a circle as the initial survey, calculating the temperature gradient in the azimuthal direction around the circle. The average of the temperatures at the two locations along the circle where the temperature gradient peaks can be used as the isotherm temperature that the AUV selects to track along. This azimuthal temperature gradient front detection method has not been applied in the virtual front tracking experiments described in this paper, however it will be integrated into future iterations of BHV_FrontTrackNoBdry.

IV. 3D Front Tracking

Including the third (vertical) dimension in characterizing a front is important due to features that occur in the vertical water profile, such as thermoclines, pycnoclines, Chlorophyll maxima, etc. Using a single AUV executing an adaptive horizontal helix behavior (BHV_FrontTrackHelix) along the front line and with the central axis at a fixed depth, the front through that depth can be estimated as a plane.

Multiple AUVs may also be employed, each at a different depth, but roughly vertically aligned, to create a 3D map of a front. Each AUV would independently perform either 2D adaptive zigzag front tracking or 3D adaptive helix front tracking, while a separate behavior would be designed to keep them roughly stacked vertically. This, however, is beyond the scope of this paper and will not be addressed further here.

The 3D, single-AUV front tracking behavior designed here, BHV_FrontTrackHelix, is based on the same weighted linear least squares estimation of the front line at a given depth that is used in the adaptive front tracking zigzag behavior, but the AUV's position is guided by a horizontal helix around the chosen depth's front line. In designing this behavior for an AUV, the helix characteristics are constrained by:

- the AUV's speed,
- the AUV's maximum ascent angle ($\sim 30^\circ$),
- the desired helix radius (manually selected based on water depth and depth of AUV),
- and the front line estimate at the helix's center depth.

The AUV's desired position on the helix at the current time, (x, y, z, t_{now}), is calculated considering the constraints above. Details of this calculation can be found in Chapter 5 of [19].

Section V describes the resulting virtual experiments and data collected from testing the 2D and 3D front tracking behaviors described above.

V. Virtual Experiments & Results

In order to compare preplanned front mapping missions to adaptive front tracking missions, a number of virtual experiments were run with one AUV performing a fixed preplanned horizontal zigzag while a second AUV used adaptive front tracking behaviors to track the front it detected. The AUV conducting the fixed preplanned zigzag shared its start location with that of the adaptive AUV. The heading, amplitude, and period of the preplanned zigzag were selected based on operator estimation of the front position from a random snapshot of the front at the AUVs' operational depth. All AUVs were assigned the same operational depth (or helix center-axis depth) in a given virtual experiment, and the virtual experiments ended when the fixed zigzag mission finished or the virtual experiment exceeded a specified amount of time (for comparative missions not involving the fixed zigzag mission). The performance of fixed zigzag and adaptive front tracking missions was evaluated and compared using a number of performance metrics, which are described in Section VI-A. A 4D MSEAS ocean model integrated into the MIT

Petillo S., H. Schmidt, P.F.J. Lermusiaux, D. Yoerger and A. Balasuriya, 2015.
"Autonomous & Adaptive Oceanographic Front Tracking On Board Autonomous Underwater Vehicles."
Proceedings of IEEE OCEANS'15 Conference, Genoa, Italy, 18-21 May, 2015.

Laboratory for Autonomous Marine Sensing Systems (LAMSS) AUV virtual experiment environment, described in Section V-A, was used as a realistic oceanographic environment for testing the behaviors described in Sections III and IV.

A. MSEAS 4D Ocean Model Environment

The MSEAS group at MIT uses oceanographic data coupled with fluid dynamics and physical oceanography principles to create 4D, spatiotemporally dynamic, gridded ocean models [20]. These models are provided in NetCDF format with a number of tools written in MATLAB to read, interpolate, and plot the model data. MSEAS models were incorporated into the LAMSS AUV virtual experiment setup to provide a realistic testing environment for the environmentally adaptive feature tracking missions, including data extraction and visualization tools.

a) Model Selection for Virtual Experiments: For the application of front tracking, the Mid-Atlantic Bight (MAB) region was selected for the shelfbreak front off the Atlantic coast of the U.S. and the robust model available for this region. The data input to the MAB model were from the real-time Shallow Water 2006/Autonomous Wide Aperture Cluster for Surveillance (SW06/AWACS) exercise that was carried out in the New Jersey Shelf/Hudson Canyon region over the time period August–September 2006 [24]–[28].

The environmental parameters available in this MSEAS model are temperature, T, salinity, S, and zonal, meridional, and vertical currents, u, v, and w, respectively, at each grid point, ($Longitude$, $Latitude$, $Depth$, $time$). The shelfbreak front is most apparent when looking at salinity (see Fig. 4), but it is also relatively clear in the temperature signature [1]. Since many temperature sensors are more robust than salinity sensors, temperature is used as the parameter that guides the decisions in the front tracking behaviors. However, *accurate* salinity, density, or sound speed measurements can also be used as input to the same front tracking algorithms when they are frontal indicators.

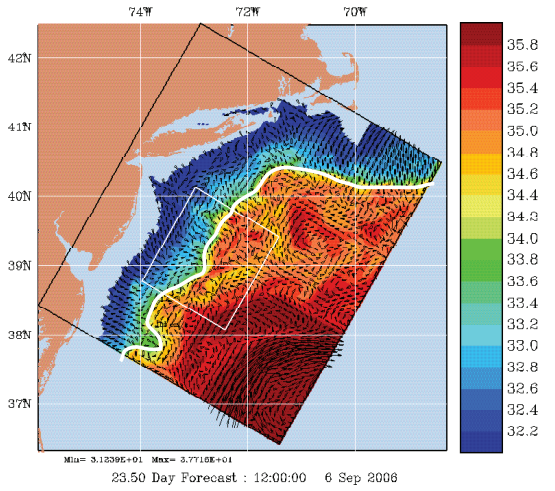

Fig. 4. A horizontal slice of the MSEAS SW06 model data for the Mid-Atlantic Bight region. The shelfbreak thermal and salinity front is highlighted in white through the Mid-Atlantic Bight region. The color variations indicate the salinity values. The SW06 domain is the full domain bounded by the black-bordered box. Adapted from [28].

b) AUV Operation Region: Within the model SW06 domain, two AUV operation boxes were defined in the area where the Pioneer Array is planned to be deployed with AUVs and gliders at the shelfbreak. In this region, the model has 3 km horizontal grid resolution. There is a distinct thermal and salinity front present along the entire shelfbreak, highlighted in Fig. 4, that was used for testing the front tracking behaviors described in Sections III and IV.

B. Preplanned Missions

The preplanned mission used in the virtual experiments consisted of a zigzag across a straight line. The straight-line zigzag was at constant depth and heading with a fixed amplitude, period, and number of straight leg segments. The isothermal contour position was assumed to be known and static for planning purposes (taken from a random snapshot of a horizontal slice at the AUVs' operational depth), but a large coverage area was selected for the survey to maximize sampling distance across the front and minimize loss of the front line. Since a snapshot of the temperatures at depth was used to determine the position and size of the preplanned mission, the resulting survey area covered by this mission does not always reflect the position of the dynamic front over time.

C. New Adaptive Missions

The adaptive front tracking missions task a single AUV with detecting and tracking an isothermal contour representing the front line, using temperature measurements it collects *in situ*. The AUV runs either the 2D (BHV_FrontTrackNoBdry) or 3D (BHV_FrontTrackHelix) front tracking behavior to keep it tracking the front locally. For 2D front tracking, the AUV attempts to track along the front in horizontal space, crossing the front locally at an $\sim 45^{\circ}$ angle to the front line. Since there is a fixed distance traveled before the AUV turns around to re-cross the front, the resulting motion under ideal conditions creates an approximately constant amplitude zigzag pattern that travels along the front boundary as the front shifts its location in time and space (see Fig. 5). Good front tracking conditions generally consist of low currents in horizontal space, such that the front doesn't move faster than the AUV can follow, and a gradually curving front line lacking isolated pockets of high or low temperatures.

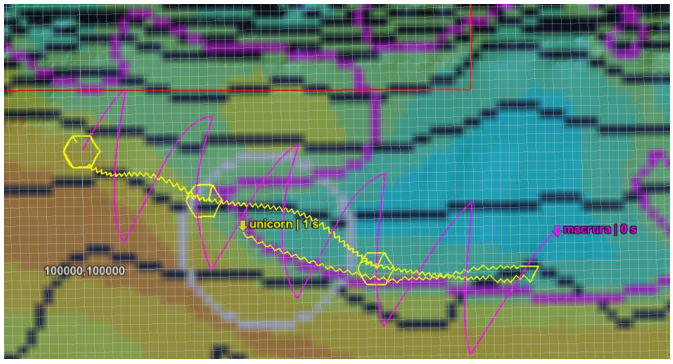

Fig. 5. An adaptive 2D front tracking mission with nearly ideal front tracking at constant depth. The adaptive AUV path is the yellow '*Unicorn*' line and the preplanned AUV path is the magenta '*Macrura*' line, while the frontal isotherm location is highlighted (at the time of this snapshot) in purple.

When conditions are poor for front tracking, the AUV's adaptive front tracking motion tends to yield more clusters of overlapping loiter patterns, as seen in Fig. 6. This occurs most frequently when the front line curves sharply or creates a closed loop on the order of 10 km or less, or when horizontal currents are strong enough to move the front line away from the AUV faster than the AUV can move.

In the case of 3D front tracking, a single AUV follows a helical path with the helix axis locally centered about a fixed-depth frontal isotherm. Under good tracking conditions, the resulting AUV path will largely look like a meandering slinky. However, under bad 3D front tracking conditions, the AUV spends most of its time loitering at constant depth to try to determine where the local front line is, similar to poor 2D front tracking runs.

Petillo S., H. Schmidt, P.F.J. Lermusiaux, D. Yoerger and A. Balasuriya, 2015.
"Autonomous & Adaptive Oceanographic Front Tracking On Board Autonomous Underwater Vehicles."
Proceedings of IEEE OCEANS'15 Conference, Genoa, Italy, 18-21 May, 2015.

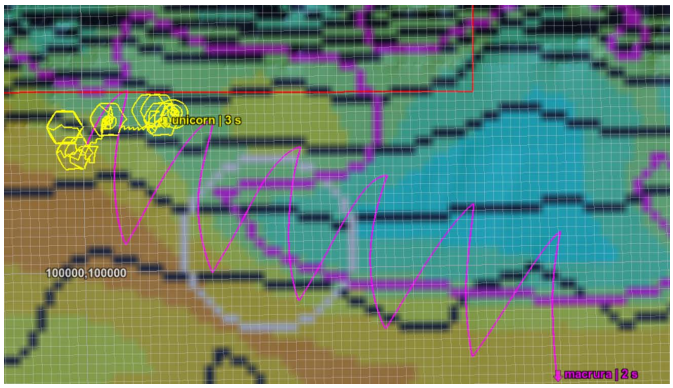

Fig. 6. An adaptive 2D front tracking mission with poor front tracking at constant depth. The adaptive AUV path is the yellow '*Unicorn*' line and the preplanned AUV path is the magenta '*Macrura*' line, while the frontal isotherm location is highlighted (at the time of this snapshot) in purple.

D. Mission Configurations

This section details the specific virtual experiment mission configurations used to test the adaptive missions in various configurations and evaluate the adaptive missions against the preplanned missions. The dynamics model for Bluefin AUVs was used for all AUVs in all virtual experiments in order to keep the AUV dynamics constant. *Unicorn* and *Macrura* were the two AUVs selected to run missions in each virtual experiment. The virtual experiments and their configurations, goals, and missions for each AUV are summarized below.

- **Runs 24–31:** 3D, 2-AUV, 1 adaptive zigzag & 1 adaptive helix, vary depth & helix dimensions (4 virtual experiments)
- **Runs 36–64:** 2D, 2-AUV, 1 adaptive & 1 preplanned, constant amplitude and depth, comparative: adaptive & preplanned straight zigzag (29 virtual experiments)

VI. Analysis

All virtual experiment runs listed at the end of Section V-D will be qualitatively and quantitatively analyzed here using a number of performance metrics and observations of the missions' performance. For the large batch of 2-AUV virtual experiments comparing the 2D adaptive front tracking behavior to the preplanned straight zigzag behavior (Runs 36–64), the overall improvement (or lack thereof) of the adaptive missions over the preplanned ones will also be quantified.

A. Performance Metrics

A number of performance metrics have been developed to evaluate and compare the front sampling ability of both preplanned and adaptive AUV front tracking missions. The variables measured during the front tracking missions and used to calculate these metrics are defined in Table I and Eqs. 1–5.

$$v_{avg} = \frac{1}{N_{spd}} \sum_{i=1}^{N_{spd}} (v_{nav})_i \tag{1}$$

$$D_{total} = \sum_{i=1}^{N_{pos}} \sqrt{(x_i - x_{i-1})^2 + (y_i - y_{i-1})^2} \tag{2}$$

$$D_{front} = t_{mission} v_{avg} \cos(\theta) \tag{3}$$

$$D_{from\_front} = \frac{-a_1 x + y - a_0}{\sqrt{(a_1^2 + 1)}} \tag{4}$$

TABLE I
Variables used to calculate performance metrics.

Variable	Significance
$t_{mission}$	Total mission time
v_{avg}	Average AUV speed (Eq. 1)
v_{nav}	Actual AUV speed at a given time (sample)
N_{spd}	Total number of AUV speed sample points
θ	Front intersect angle
D_{total}	Total distance traveled (Eq. 2)
N_{pos}	Total number of AUV position locations
D_{front}	Total possible distance AUV could have tracked along front, given $t_{mission}$. Estimated by the best-case calculation (AUV perfectly tracks the front, crossing the front at an angle of θ). (Eq. 3)
D_{on_front}	Distance AUV tracked along the front line ($\leq D_{front}$)
N_{cross}	Number of front crossing points, total, while tracking front
D_{from_front}	Perpendicular distance (closest point of approach) from AUV position, (x, y), to front estimate line (Eq. 4)
a_1 and a_0	The slope and intercept, respectively, of the front line estimate in the local x-y grid
$\partial T/\partial r$	Temperature (T) gradient in the across-front direction, relative to the front estimate line (Eq. 5)
N^+	Number of above-average $\partial T/\partial r$ bins
N_{tot}	Total number of $\partial T/\partial r$ bins

$$\frac{\partial T}{\partial r} = \frac{\partial T}{\partial D_{from\_front}} \tag{5}$$

The performance metrics equations derived from the variables above are summarized in Table II and are as follows:

ρ = Crossing Density; i.e., how many front crossings were made by the AUV per unit length of the front line that was tracked.

D_{cross} = Distance between Crossings; i.e., the average distance the AUV traveled between front crossings.

ϵ = Front Sampling Efficiency; i.e., the percentage of D_{front} that was tracked and sampled by the AUV.

ER = Excess Ratio; i.e., how much of the AUV's travel distance was in excess of the distance along the front that the AUV captured the front.

FEE = Front Estimate Error, which compares the $|\partial T/\partial r|_{max}$ location to the local estimated front location, as captured by the AUV.

TC = Tracking Confidence, which is an evaluation of the confidence level indicating whether the actual front was followed/sampled by the AUV, expressed as a percentage. The scaling factor of 2 accounts for the fact that most $\partial T/\partial r$ sample bins have below-average values, and a minority of samples have above-average values due to sharp peaks in $\partial T/\partial r$ in the across-front direction, so at best it would be expected to see $N^+/N_{tot} = 0.5$.

Based on the performance metrics defined in Eqns. 6-11 in Table II, higher Crossing Density (ρ) and Sampling Efficiency (ϵ) values indicate better performance tracking along the front, while higher Distance between Crossings (D_{cross}) and Excess Ratio (*ER*) values indicate worse performance. It is often desirable to maintain some across-front motion of the AUV as well, thus extremes of huge ρ and tiny D_{cross} and *ER* values are not always optimal. Sailing along the front is good, but in many cases, crossing the front frequently is also good.

B. Data Analysis

1) Runs 36–64: 2D, comparing adaptive & preplanned straight zigzag front tracking: Virtual experiment Runs 36–64

Petillo S., H. Schmidt, P.F.J. Lermusiaux, D. Yoerger and A. Balasuriya, 2015.
"Autonomous & Adaptive Oceanographic Front Tracking On Board Autonomous Underwater Vehicles."
Proceedings of IEEE OCEANS'15 Conference, Genoa, Italy, 18-21 May, 2015.

TABLE II
SUMMARY OF PERFORMANCE METRICS EQUATIONS.

Performance Metric	Equation	Better Values	Significance
Crossing Density [crossings/m]	$\rho = \frac{N_{cross}}{D_{on\_front}}$ (6)	higher*	How many front crossings were made by the AUV per unit length of the front line that was tracked
Distance between Crossings [m/crossing]	$D_{cross} = \frac{1}{\rho}$ (7)	lower*	The average distance the AUV traveled between front crossings
Sampling Efficiency [%]	$\epsilon = \frac{D_{on\_front}}{D_{front}} \times 100\%$ (8)	higher	The percentage of D_{front} that was tracked and sampled by the AUV
Excess Ratio	$ER = \frac{D_{total}}{D_{on\_front}}$ (9)	lower*	How much of the AUV's travel distance was in excess of the distance along the front that the AUV captured the front
Front Estimate Error [m]	$FEE = D_{from\_front}@\lvert\partial T/\partial r\rvert_{max}$ on a zigzag leg (10)	lower	Compares the $\lvert\partial T/\partial r\rvert_{max}$ location to the local estimated front location, as captured by the AUV
Tracking Confidence [%]	$TC = 2\left(\frac{N^+}{N_{tot}}\right) \times 100\%$ (11)	higher	An evaluation of the confidence level indicating whether the actual front was followed/sampled by the AUV, expressed as a percentage

* It is often desirable to maintain some across-front motion of the AUV, thus extremes of these values are not always optimal.

were designed to determine a baseline of performance for 2D adaptive front tracking versus preplanned straight zigzag front sampling. A quantitative analysis of preplanned versus adaptive missions has been performed for the case of single AUVs doing 2D front tracking. The *Unicorn* AUV was tasked with 2D adaptive front tracking, while the *Macrura* AUV was given a preplanned fixed zigzag pattern to execute. In all cases, both *Unicorn* (adaptive) and *Macrura* (preplanned) started at the same location and executed their paths over the same mission duration. *Macrura*'s preplanned path was selected to cover the general location of the front near the MAB shelfbreak. *Unicorn*'s adaptive zigzag was configured based on the spatiotemporal scales of the front and the speed limitations of the AUV.

With this setup, 29 missions were completed with both AUVs starting at (100000 m, 113000 m) relative to two Datum locations: (38.6°N, -71.9°E) and (39.409291°N, -71.934359°E). The former (more southerly) Datum location corresponded with a fixed zigzag heading of 109°, while the latter Datum required a fixed zigzag heading of 101° to accommodate the slight change in general heading of the front north of the shelfbreak. The various performance metric variables were tracked while the virtual experiments were running and, after the fact, the performance metrics themselves were calculated and plotted for both AUVs in post-processing. These results are shown in Fig. 7, where each color represents a different set of virtual experiment runs. In order to keep as many parameters constant as possible, the AUV running the preplanned zigzag (*Macrura*) tracked its front crossings based on the frontal temperature that the adaptive AUV (*Unicorn*) determined for front tracking.

Based one the performance metrics defined in Eqns. 6-9, higher Crossing Density (ρ) and Sampling Efficiency (ϵ) values indicate better performance, while higher Distance between Crossings (D_{cross}) and Excess Ratio (*ER*) values indicate worse performance. In the case of this set of virtual experiments, for all performance metrics, the adaptive front tracking algorithms are generally an improvement over using a preplanned zigzag mission for collecting data along a front.

Additionally, Tracking Confidence (*TC*) was evaluated for the adaptive missions based on temperature data binned (by distance from the front line estimate, into 1 m bins) over entire missions. The average *TC* for the adaptive front tracking mission in Runs 36–64 was 59.2%, with a standard deviation of 9.5%. The Tracking Confidence values, along with the Front Estimate Errors (*FEE*; averaged over the FEE_{leg} calculated for each leg in a run) for the adaptive front tracking missions in each run are plotted in Fig. 8. For 28/29 (96.6%) of the runs, the magnitude of the mean *FEE* was less than 400 m (100% had magnitudes less than 800 m), which is relatively small compared to the O(10 km) horizontal spatial scale of the MAB shelfbreak front. The low *FEE* values mean that the adaptive AUV did a good job covering the actual front interface ($\lvert\partial T/\partial r\rvert_{max}$) while staying close to the estimated front line when tracking the front, and the middling *TC* values (greater than 40% for all of the runs, greater than 50% for 82.8% the runs, greater than 70% for 13.8% of the runs) mean that the adaptive AUV sampled close to the front interface in at least 25% of the temperature (and thus $\lvert\partial T_{binned}/\partial r\rvert$) bins in 82.8% of the runs.

For the *TC* and *FEE* values, it is important to note that the distances represented by these values (O(100 m)) are much smaller than the 3 km resolution of the ocean model being used for these virtual experiments. Since the data in the model are linearly interpolated between the grid points, it is not fully representative of the smaller scale variations in temperature that would be observed in the real ocean, and thus these *TC* and *FEE* values may not be not accurate in real ocean environments (or higher-resolution models). However, these values are accurate for data smoothed or gridded to approximately 3 km resolution, as was used here. In order to get more accurate *TC* and *FEE* results for higher-resolution and real ocean environments, improvements are still needed to the 2D adaptive front tracking behavior to make it successful in these environments.

2) Runs 24–31: 3D, adaptive zigzag vs. adaptive helix: Runs 24–31 evaluated the 3D adaptive helix front tracking mission against the 2D adaptive zigzag front tracking mission. For these runs,

Petillo S., H. Schmidt, P.F.J. Lermusiaux, D. Yoerger and A. Balasuriya, 2015.
"Autonomous & Adaptive Oceanographic Front Tracking On Board Autonomous Underwater Vehicles."
Proceedings of IEEE OCEANS'15 Conference, Genoa, Italy, 18-21 May, 2015.

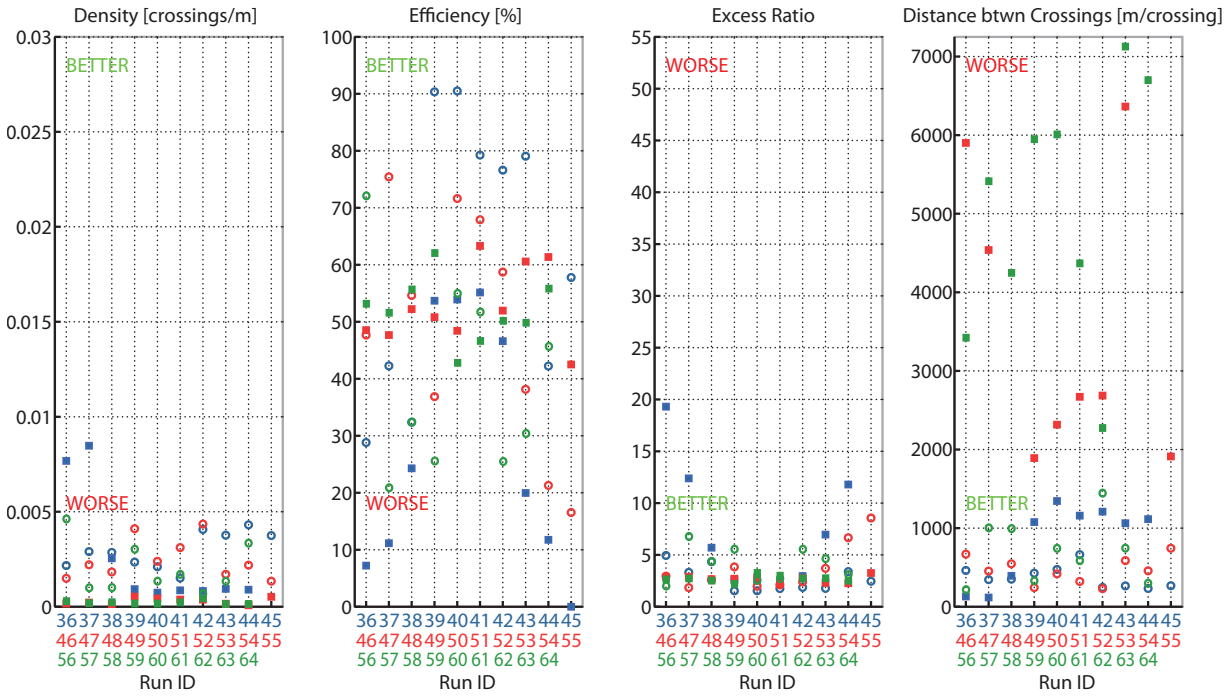

Fig. 7. Runs 36–64: Performance metrics for *Macrura*'s preplanned zigzag missions (filled squares) and *Unicorn*'s 2D adaptive front tracking missions (open circles), plotted for each virtual experiment run. Datum: Runs 36–45 at (38.6°N, -71.9°E), Runs 46–64 at (39.409291°N, -71.934359°E). Preplanned zigzag heading: Runs 36–45 at 109°, Runs 46–64 at 101°. Better and worse values for each performance metric are indicated.

Unicorn was assigned to the 2D adaptive zigzag mission and *Macrura* to the 3D adaptive helix mission. These missions were centered at four different depths, and the helix radius was set equivalent to its center depth while the spacing between helix loops was set to four times the helix radius (to maintain 45° front intersect angles). The center depths selected for the virtual experiments were 30 m (Runs 24 & 28), 100 m (Runs 25 & 29), 300 m (Runs 26 & 30), and 1000 m (Runs 27 & 31). Each different depth-centered set of missions was evaluated at two model time ranges. See Fig. 9 for all performance metrics results.

For most of these runs, the 3D adaptive helix showed reduced performance (lower Efficiency, higher Excess Ratio, and—for half of the runs—reduced crossing Density) when compared to the 2D adaptive zigzag, with the lowest Efficiency and greatest Excess while the helix was centered at 1000 m, due to the AUV frequently straying too far from the front over the period of one helix loop. The highest sampling Densities and smallest Distances between Crossings for the helix, however, occurred during the runs centered at 30 m and 1000 m. For the helix centered at 30 m this was actually a significant improvement over the 2D zigzags, since the helix tracked the front better with a smaller (30 m) radius (analogous to a smaller adaptive zigzag amplitude) than the adaptive zigzag with a 500 m amplitude and thus collected a denser sampling of front data. In the case of the helix centered at 1000 m having comparatively higher Densities and smaller Distances between Crossings than the 2D adaptive zigzags, this apparent improvement in performance comes with the caveat that the helix was continuously losing the front line and returning to the last detected front crossing location (thus finding a 'new' crossing point right next to the previous one) after re-starting the helix motion, rather than performing the helix behavior to its full extent. This resulted in a glut of front crossings within a small area for the helix centered at 1000 m, but very little tracking along the front using the helix, resulting in very poor performance despite the seemingly good Density and Distance between Crossings metrics.

This overall reduction in performance from the 2D to the 3D adaptive front tracking is expected, given that the 3D helix requires the AUV to travel a longer path (changing depth) as it crosses the front, rather than gathering many points at the fixed helix-center depth. Since fewer points are available to the 3D adaptive helix behavior to determine the presence and location of a front crossing point at the helix-center depth (there may be as few as two points at the center depth on a given rotation of the AUV around the helix) than there are for the 2D adaptive zigzag behavior at constant depth, there is higher risk of the helix losing the front location as it travels through depth. For the runs centered at 30 m, 100 m, and 300 m, in fact, the reduction in performance is somewhat balanced by the data set being collected, which is 3-dimensional in space rather than just 2-dimensional. The 3D data set collected by the helix captures the distribution of temperature with depth, making it possible to approximate the front's structure as a plane in 3D space rather than just as a 2D line. This means it is possible to successfully collect a 3D spatial distribution of temperature along the front using this horizontal helix front tracking behavior without the need for a second AUV, with the concession of a slight reduction in performance compared to the 2D adaptive zigzag behavior.

VII. Conclusion

The goals of the work presented in this paper were to apply AAEA and Feature Tracking to adaptively sample along and across an ocean front using only the data collected on board AUVs, gathering a synoptic data set of the position of the front over time while improving sampling efficiency and density over current preplanned AUV sampling surveys.

To this end, two adaptive autonomy behaviors were developed for front tracking in 2D and 3D space, with single AUVs: BHV_FrontTrackNoBdry (2D front-following zigzag) and BHV_FrontTrackHelix (3D front-following helix). A number of performance metrics were developed for comparative evaluation of these

Petillo S., H. Schmidt, P.F.J. Lermusiaux, D. Yoerger and A. Balasuriya, 2015.
"Autonomous & Adaptive Oceanographic Front Tracking On Board Autonomous Underwater Vehicles."
Proceedings of IEEE OCEANS'15 Conference, Genoa, Italy, 18-21 May, 2015.

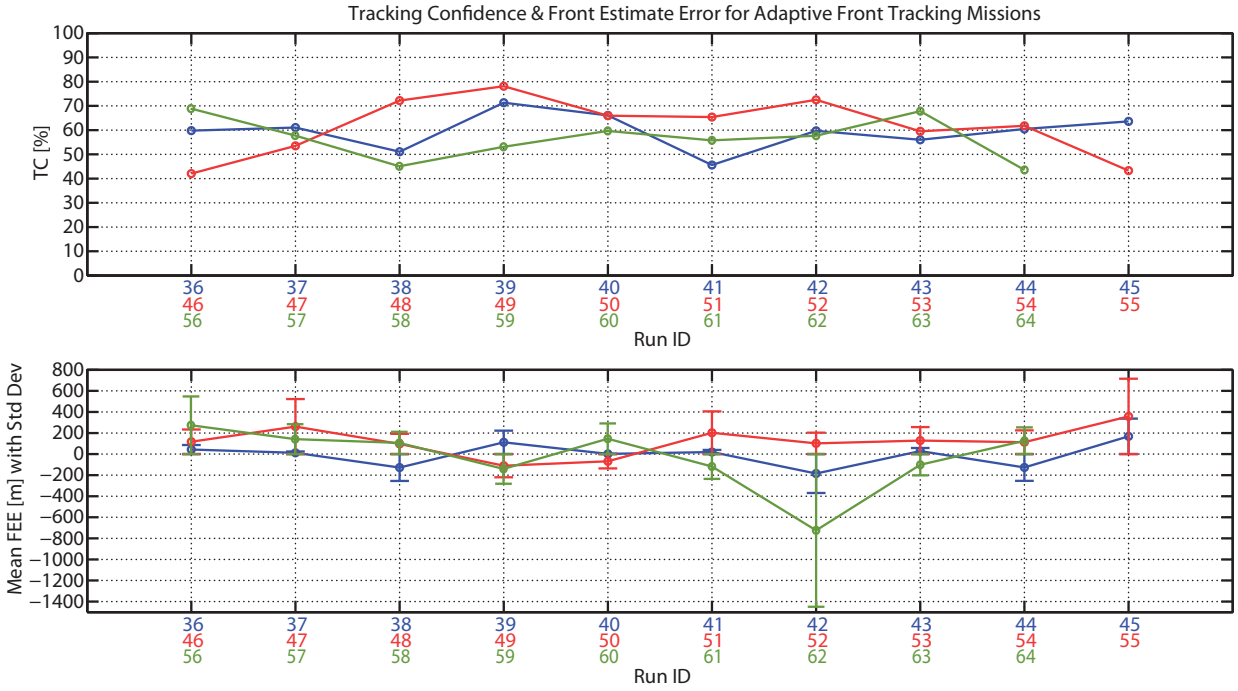

Fig. 8. Runs 36–64: Tracking Confidence and average Front Estimate Errors for *Unicorn*'s 2D adaptive front tracking missions, plotted for each virtual experiment run. The *TC* was calculated from spatially-binned temperature data over entire runs. The *FEE* was averaged over the FEE_{leg} calculated for each leg in a run, and the standard deviations are plotted here as error bars around the mean values. Datum: Runs 36–45 at (38.6°N, -71.9°E), Runs 46–64 at (39.409291°N, -71.934359°E). Preplanned zigzag heading: Runs 36–45 at 109°, Runs 46–64 at 101°.

behaviors. The 2D front tracking behavior's performance was also evaluated against that of a preplanned zigzag survey (representative of current methods used for collecting data along a front). A spatiotemporally dynamic MSEAS model of the Mid-Atlantic Bight region off the east coast of the U.S. was used as a testing environment for virtual experiments, allowing these new AUV front tracking methods to be evaluated.

The front tracking behaviors presented here are essentially isotherm-following behaviors, since the across-front temperature gradient can vary in the along-front direction and the uncertain angle at which an AUV crosses the front and samples the temperature would affect the apparent temperature gradient at a given location. The front tracking behaviors use a three-phase process (conceptualized in Fig. 3) to achieve front isotherm tracking: detection, classification, and tracking.

Overall, the 2D adaptive front tracking behavior presented here succeeded in improving front mapping performance over that of a preplanned straight zigzag pattern at least 58% of the time in virtual experiments (Runs 36–64: adaptive vs. preplanned straight zigzag). The performance metrics used to evaluate the adaptive and preplanned front tracking behaviors are summarized in Table II. Adaptive front tracking had the largest and most consistent impact on front Crossing Density (ρ) and Distance between Crossings (D_{cross}), where it was an improvement over the preplanned straight zigzag 89.7% of the time. Adaptive front tracking showed less stark Sampling Efficiency (ϵ) and Excess Ratio (*ER*) improvements over the preplanned straight zigzag, displaying improved numbers 62.1% and 58.6% of the time, respectively. It is also apparent that the start location of the front tracking missions affects the performance of adaptive versus preplanned front tracking. When the front tracking missions were moved north onto the shelf from the original mission area south of the shelfbreak, the adaptive front tracking algorithms tended to track the front worse than the preplanned zigzag despite the stronger across-front temperature gradient in the more northerly location. This was due to a mesoscale slope-water eddy surrounded by an isotherm of the same temperature as the front that *Unicorn* (adaptive AUV) was stuck in while trying to track along the front north of the MAB shelfbreak. The average Tracking Confidence (*TC*) for the adaptive front tracking missions in Runs 36–64 was calculated as 59.2%, with a standard deviation of 9.5%, suggesting that the actual shelfbreak front is usually sampled in 25%-34% of the range bins around the estimated front line. For the majority of the runs, the adaptive mission's Front Estimate Error (*FEE*) value was under 400 m, with standard deviations mostly under 150 m, suggesting that the adaptive AUV tracked fairly close to the actual front line. It is important to note here that the *TC* and *FEE* values are only valid for 3 km resolution environments with interpolation between grid points and may not be valid for higher-resolution models or the actual ocean environment without further improvements to the front tracking behavior.

Runs 24–31 (2D adaptive zigzag vs. 3D adaptive helix) suggest a general reduction in front tracking performance when using the 3D adaptive horizontal helix compared to the 2D adaptive zigzag, except when using the helix centered at 30 m. This reduction in performance is due to—and somewhat balanced by—the fact that the helix is also collecting data over a continuous depth range (rather than just one depth) along and across the front. That is, the 2D adaptive zigzag behavior collects all of its data points at a constant depth (thus, it has a lot of data at the depth at which it is determining the front), whereas the 3D adaptive helix behavior may have as few as two points collected at its center depth (at which it is determining the front) per period of travel around the helix, making the helical front tracking much more sensitive to spurious data values or smaller-scale temperature variations than the zigzag front tracking at constant depth. The 3D motion of the helix will, however, allow the front to be approximated (in future work) as a plane instead of just a line, and it adds a depth dimension to the coverage of the front where helical front tracking occurs.

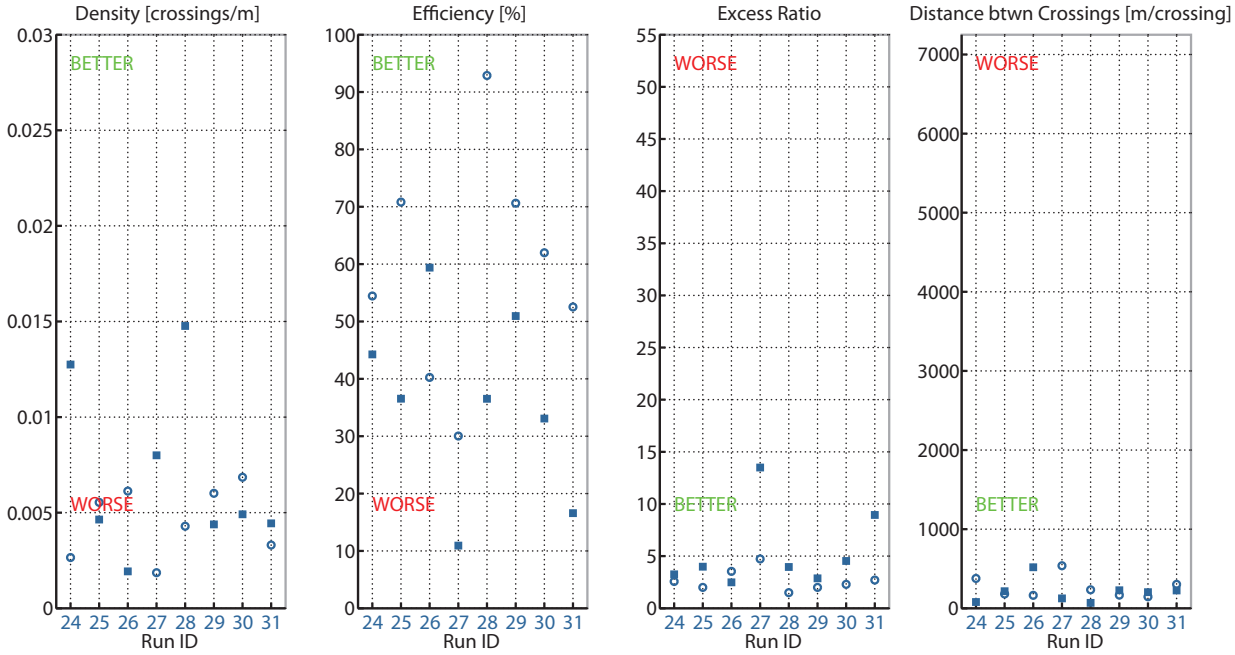

Fig. 9. Runs 24–31: Performance metrics for *Macrura*'s 3D adaptive helix front tracking missions (filled squares) and *Unicorn*'s 2D adaptive zigzag front tracking missions (open circles), plotted for each virtual experiment run. Each different depth-centered set of missions was evaluated at two model time ranges. Better and worse values for each performance metric are indicated.

Ultimately, the added complexity of using adaptive front tracking to sample along a front must be weighed against the amount of human-AUV interaction and resources necessary to deploy a pre-planned AUV survey for the the same purpose. Preplanned surveys require a significant amount of operator interaction, data processing, and mission planning between AUV dives to collect the desired data set. As a counterpoint, adaptive front tracking only requires the operator or researcher to have a rough idea of where a front might be, as the AUV will determine the exact location and follow the front itself, requiring no shipboard data processing and no redeployment or planning of new missions to maintain sampling along the front. This significantly reduces the time the AUV spends not tracking the front (i.e., on the surface awaiting redeployment or conducting a much larger amplitude zigzag to ensure frontal coverage) and frees up a ship's resources for other scientific experiments to be performed simultaneously. In conclusion, autonomous and adaptive front tracking techniques add up-front complexity to an AUV's software, but, once implemented, significantly reduce the labor and uncertainty involved in efficiently gathering a synoptic data set characterizing an oceanographic front, making the use of autonomous and adaptive front tracking methods worthwhile.

Acknowledgment

Financial support of this work was provided by the U.S. Office of Naval Research (award # N00014-11-1-0097) GOATS '11 and (award # N00014-14-1-0214) GOATS '14 projects - Adaptive and Collaborative Exploitation of 3-Dimensional Environmental Acoustics in Distributed Undersea Networks.

The authors would like to thank Dr. Toby Schneider for helping with all of the code tweaks and extra features that made the virtual experiments in this paper easier to visualize and possible to run, Dr. Michael Benjamin for writing and maintaining the IvP Helm and for contributing computing power, which have made the many months of virtual experiments in this paper possible, Dr. Patrick Haley Jr. for working hard to provide the MSEAS model subsets and associated information necessary for this work on short notice, and Prof. Paul Newman for writing and maintaining the MOOS project.

References

[1] R. He, K. Chen, T. Moore, and M. Li, "Mesoscale variations of sea surface temperature and ocean color patterns at the Mid-Atlantic Bight shelfbreak," *Geophysical Research Letters*, vol. 37, no. 9, pp. n/a–n/a, 2010. [Online]. Available: http://dx.doi.org/10.1029/2010GL042658

[2] N. Leonard, D. Paley, F. Lekien, R. Sepulchre, D. Fratantoni, and R. Davis, "Collective motion, sensor networks, and ocean sampling," *Proceedings of the IEEE*, vol. 95, no. 1, pp. 48–74, Jan 2007.

[3] P. F. J. Lermusiaux, "Adaptive modeling, adaptive data assimilation and adaptive sampling," *Physica D: Nonlinear Phenomena*, vol. 230, no. 1, pp. 172–196, 2007.

[4] P. Lermusiaux, T. Lolla, P. H. Jr., K. Yigit, M. Ueckermann, T. Sondergaard, and W. Leslie, *Springer Handbook of Ocean Engineering: Autonomous Ocean Vehicles, Subsystems and Control*. Springer, Berlin, Heidelberg, 2015, ch. 11: Science of Autonomy: Time-Optimal Path Planning and Adaptive Sampling for Swarms of Ocean Vehicles, in press.

[5] N. Roy, H.-L. Choi, D. Gombos, J. Hansen, J. How, and S. Park, "Adaptive observation strategies for forecast error minimization," in *Computational Science - ICCS 2007*, ser. Lecture Notes in Computer Science, Y. Shi, G. D. van Albada, J. Dongarra, and P. M. Sloot, Eds. Springer Berlin Heidelberg, 2007, vol. 4487, pp. 1138–1146. [Online]. Available: http://dx.doi.org/10.1007/978-3-540-72584-8_149

[6] D. Paley, F. Zhang, and N. Leonard, "Cooperative control for ocean sampling: The glider coordinated control system," *Control Systems Technology, IEEE Transactions on*, vol. 16, no. 4, pp. 735–744, July 2008.

[7] S. Ramp, R. Davis, N. Leonard, I. Shulman, Y. Chao, A. Robinson, J. Marsden, P. Lermusiaux, D. Fratantoni, J. Paduan, F. Chavez, F. Bahr, S. Liang, W. Leslie, and Z. Li, "Preparing to predict: The second autonomous ocean sampling network (AOSN-II) experiment in the monterey bay," *Deep Sea Research Part II: Topical Studies in Oceanography*, vol. 56, no. 3–5, pp. 68–86, 2009, AOSN II: The Science and Technology of an Autonomous Ocean Sampling Network. [Online]. Available: http://www.sciencedirect.com/science/article/pii/S0967064508002609

[8] T. B. Curtin and J. G. Bellingham, "Progress toward autonomous ocean sampling networks," *Deep Sea Research Part II: Topical Studies in Oceanography*, vol. 56, no. 3–5, pp. 62–67, 2009, AOSN II: The Science and Technology of an Autonomous Ocean Sampling Network. [Online]. Available: http://www.sciencedirect.com/science/article/pii/S0967064508002531

[9] T. Lolla, M. Ueckermann, K. Yigit, J. Haley, P.J., and P. Lermusiaux, "Path planning in time dependent flow fields using level set methods," in *Robotics and Automation (ICRA), 2012 IEEE International Conference on*, May 2012, pp. 166–173.

[10] T. Lolla, P. Lermusiaux, M. Ueckermann, and J. Haley, PatrickJ., "Time-optimal path planning in dynamic flows using level set equations: Theory and schemes," *Ocean Dynamics*, vol. 64, no. 10, pp. 1373–1397, 2014. [Online]. Available: http://dx.doi.org/10.1007/s10236-014-0757-y

[11] T. Lolla, J. Haley, PatrickJ., and P. Lermusiaux, "Time-optimal path planning in dynamic flows using level set equations: Realistic applications," *Ocean Dynamics*, vol. 64, no. 10, pp. 1399–1417, 2014. [Online]. Available: http://dx.doi.org/10.1007/s10236-014-0760-3

[12] H. Schmidt, J. Bellingham, M. Johnson, D. Herold, D. Farmer, and R. Pawlowicz, "Real-time frontal mapping with auvs in a coastal environment," in *OCEANS '96. MTS/IEEE. Prospects for the 21st Century. Conference Proceedings*, vol. 3, Sep 1996, pp. 1094–1098 vol.3.

[13] E. Fiorelli, N. Leonard, P. Bhatta, D. Paley, R. Bachmayer, and D. Fratantoni, "Multi-AUV Control and Adaptive Sampling in Monterey Bay," *Oceanic Engineering, IEEE Journal of*, vol. 31, no. 4, pp. 935–948, Oct 2006.

[14] D. Wang, P. F. Lermusiaux, P. J. Haley, D. Eickstedt, W. G. Leslie, and H. Schmidt, "Acoustically focused adaptive sampling and on-board routing for marine rapid environmental assessment," *Journal of Marine Systems*, vol. 78, no. Supplement 1, pp. S393 – S407, 2009. [Online]. Available: http://www.sciencedirect.com/science/article/pii/S0924796309001675

[15] Y. Zhang, M. Godin, J. Bellingham, and J. Ryan, "Ocean front detection and tracking by an autonomous underwater vehicle," in *OCEANS 2011*, Sept 2011, pp. 1–4.

[16] ——, "Using an autonomous underwater vehicle to track a coastal upwelling front," *Oceanic Engineering, IEEE Journal of*, vol. 37, no. 3, pp. 338–347, July 2012.

[17] C. Cannell and D. Stilwell, "A comparison of two approaches for adaptive sampling of environmental processes using autonomous underwater vehicles," in *OCEANS, 2005. Proceedings of MTS/IEEE*, Sept 2005, pp. 1514–1521 Vol. 2.

[18] S. Petillo, A. Balasuriya, and H. Schmidt, "Autonomous adaptive environmental assessment and feature tracking via autonomous underwater vehicles," in *OCEANS 2010 IEEE - Sydney*, Sydney, Australia, May 2010, pp. 1–9.

[19] S. Petillo, "Autonomous & adaptive oceanographic feature tracking on board autonomous underwater vehicles," Ph.D. dissertation, Massachusetts Institute of Technology, Cambridge, MA, & Woods Hole Oceanographic Institution, Woods Hole, MA, February 2015.

[20] P. J. Haley, Jr. and P. F. J. Lermusiaux, "Multiscale two-way embedding schemes for free-surface primitive equations in the Multidisciplinary Simulation, Estimation and Assimilation System," *Ocean Dynamics*, vol. 60, no. 6, pp. 1497–1537, Dec. 2010.

[21] S. Petillo and H. Schmidt, "Autonomous and adaptive plume detection and tracking with auvs: Concepts, methods, and available technology," in *Proceedings of the 9th IFAC Conference on Manoeuvring and Control of Marine Craft*, G. Bruzzone and M. Caccia, Eds., vol. 9, Arenzano, Italy, September 2012, pp. 232–237. [Online]. Available: http://www.ifac-papersonline.net/Detailed/64611.html

[22] B. Reed and F. Hover, "Tracking ocean fronts with multiple vehicles and mixed communication losses," in *IEEE/RSJ International Conference on Intelligent Robots and Systems (IROS)*, Nov. 2013, pp. 3374–3381.

[23] R. N. Smith, Y. Chao, P. P. Li, D. A. Caron, B. H. Jones, and G. S. Sukhatme, "Planning and implementing trajectories for autonomous underwater vehicles to track evolving ocean processes based on predictions from a regional ocean model," *International Journal of Robotics Research*, vol. 29, pp. 1475–1497, October 2010. [Online]. Available: http://dx.doi.org/10.1177/0278364910377243

[24] WHOI, "Shallow Water experiment 2006," 2006, Accessed 31 October 2014. [Online]. Available: http://acoustics.whoi.edu/sw06/

[25] P. F. J. Lermusiaux, P. J. Haley, Jr., W. G. Leslie, O. Logoutov, and A. R. Robinson, "Autonomous Wide Aperture Cluster for Surveillance (AWACS): Adaptive Sampling and Search Using Predictive Models with Coupled Data Assimilation and Feedback - Harvard Page," MSEAS Sea Exercises, 2006, Accessed 31 October 2014. [Online]. Available: http://mseas.mit.edu/archive/AWACS/index_AWACS.html

[26] N. R. Chapman and J. F. Lynch, "Special issue on the 2006 Shallow Water experiment," *IEEE Journal of Oceanic Engineering*, vol. 35, no. 1, pp. 1–2, 2010.

[27] Y.-T. Lin, A. E. Newhall, T. F. Duda, P. F. J. Lermusiaux, and P. J. Haley, "Merging multiple-partial-depth data time series using objective empirical orthogonal function fitting," *IEEE Journal of Oceanic Engineering*, vol. 35, no. 4, pp. 710–721, Oct. 2010.

[28] "MSEAS re-analyses for the AWACS-SW06 exercise in the Middle Atlantic Bight region." [Online]. Available: http://mseas.mit.edu/Research/SW06/MSEAS_reanalysis/2013_May07/